phys. stat. sol. (a) **173**, 467 (1999)

Subject classification: 75.60.Lr; S11.2

Analysis of Magnetic After-Effects in Manganese Ferrites

F. WALZ (a), J. RIVAS (b), J. H. V. J. BRABERS (a), and H. KRONMÜLLER (a)

(a) Max-Planck-Institut für Metallforschung, Heisenbergstr. 1, D-70569 Stuttgart, Germany

(b) Universidade de Santiago de Compostela, Facultad de Fisica,
E-15706 Santiago de Compostela, Spain

(Received December 28, 1998)

The low-temperature ($4\,\mathrm{K} < T < 125\,\mathrm{K}$), electron-induced magnetic after-effect (MAE) spectra of vacancy-doped manganese ferrites, $Fe_{3-x-\Delta}Mn_xO_4$ ($0.002 \leq x \leq 0.8$ and $\Delta \approx 4 \times 10^{-3}$), are investigated in detail. The tunnelling-induced MAEs ($4\,\mathrm{K} < T < 35\,\mathrm{K}$) are severely affected in the presence of even smallest Mn contents ($x \leq 0.002$). The hopping regime, though strongly modified upon continued doping – i.e. by narrowing and low-temperature shifting ($\leq 50\,\mathrm{K}$) – persists over the whole concentration range. Its high-temperature collapse remains accompanied by a pronounced susceptibility jump, thus indicating preservation of a residual, second-order Verwey-like crystallographic phase transition. The vacancy-mediated process III (300 K) and its Mn-dependent satellite II ($\approx 380\,\mathrm{K}$) are quantitatively analyzed and the, also Mn-induced, process IV (200 K) interpreted in a novel way in terms of intrinsic interstitials.

Die elektronischen, im Tieftemperaturgebiet ($4\,\mathrm{K} < T < 125\,\mathrm{K}$) auftretenden magnetischen Nachwirkungsspektren von Leerstellen (Δ)-dotierten Manganferriten, $Fe_{3-x-\Delta}Mn_xO_4$, der Zusammensetzung $0{,}002 \leq x \leq 0{,}8$ und $\Delta \approx 4 \times 10^{-3}$, werden eingehend untersucht. Die typischen Tunnelprozesse, im Bereich $4\,\mathrm{K} < T < 35\,\mathrm{K}$, werden bereits durch geringste Mn-Konzentrationen ($x \leq 0{,}002$) stark beeinträchtigt. Die Hüpf-Prozesse dagegen – obwohl mit steigendem Mn-Gehalt ebenfalls deformiert und nach tiefen Temperaturen ($\leq 50\,\mathrm{K}$) verschoben – bleiben über den ganzen Konzentrationsbereich erhalten. Dabei wird ihr Hochtemperatur-Abfall von einer sprunghaften Suszeptibilitätszunahme begleitet, die auf die Fortdauer einer Verwey-ähnlichen, kristallographischen Phasenumwandlung zweiter Ordnung hinweist. Der Leerstellen-unterstützte Prozeß III (300 K) und sein Mn-abhängiger Satellit II ($\approx 380\,\mathrm{K}$) werden quantitativ analysiert und der, ebenfalls Mn-abhängige, Prozeß IV (200 K) auf neuartige Weise als Orientierungsnachwirkung intrinsischer Zwischengitteratome gedeutet.

1. Introduction

Our present report accomplishes a previous investigation of the magnetic after-effect (MAE) in polycrystalline, vacancy-doped (Δ) Mn-ferrites, $Fe_{3-x-\Delta}Mn_xO_4$ ($0.002 \leq x \leq 0.8$), [1], by extending the original temperature range ($80\,\mathrm{K} \leq T \leq 500\,\mathrm{K}$) into the low-temperature regime of $4\,\mathrm{K} < T \leq 80\,\mathrm{K}$, which during our first investigations was not available. Meantimes we have investigated a series of related spinel-type ferrites over the full temperature range ($4\,\mathrm{K} < T < 500\,\mathrm{K}$), under various experimental conditions such as, i.e., vacancy-doping [2 to 6], presence of internal stresses ([7], cf. [3 to 6]), induction of intrinsic point defects by electron-irradiation [8], doping with impurity ions like Ba^{2+} [9], Ni^{2+} [10], Zn^{2+} [11, 12], Ti^{4+} [13, 14], Ga^{2+} [15]. Against this background of experience [16] we found it interesting and necessary to provide the present results concerning the low-temperature behaviour of Mn-ferrites.

This information is of special interest since, upon cooling down, magnetite undergoes near $T_v \approx 125\,\mathrm{K}$ a first-order electronic phase transition, called after Verwey, which is accompanied by a drastic change of various intrinsic material parameters like crystal structure, conductivity, susceptibility, magnetization, etc. [17 to 19]. This transition is associated with a corresponding order change of the Fe^{2+} and Fe^{3+} ions being placed on the octahedral B-sites of the inverse spinel, whereas A-sites, in both phases, are invariably occupied by Fe^{3+} ions. Thus, only in the low-temperature phase, the B-sited Fe^{2+} and Fe^{3+} ions follow a scheme of definite long-range order ([20], cf. [5, 17 to 19]) which, together with the residual orbital momentum of the Fe^{2+} ($3d^6$) ion – in contrast to Fe^{3+} ($3d^5$) – opens the chance for electron exchange between neighboring B-site ions according to the reaction:

$$Fe^{3+} + e^- \rightleftarrows Fe^{2+} . \tag{1}$$

The driving force for such electron exchange may be seen in the concomitant local transfer of magnetic anisotropy into such positions where the ferrimagnetic system can respond by a lowering of the free enthalpy. Our preceding investigations [3 to 16] revealed, indeed, the temperature regime of the ionically ordered phase of perfect magnetite ($T < T_v$) to be governed by two characteristic relaxation processes of type (1) which could be identified as (i) incoherent tunnelling ($4\,K < T \leq 35\,K$) and (ii) thermally activated hopping ($50\,K < T < 125\,K$). Since these tunnel- and hopping-spectra are best developed in perfect crystals [3 to 8] they may be utilized as sensitive probes concerning sample quality and nature of the Verwey transition [7, 8, 16], thus providing also valuable information on the conductivity mechanisms in the material [21].

The vacancy-mediated high-temperature relaxation processes II ($T \geq 380\,K$) and III ($T \approx 300\,K$) have been studied in great detail already in our preceding paper [1] and their mechanisms explained in terms of model considerations which, thereafter, proved to be applicable as well on the corresponding MAE spectra of a variety of related magnetite-based ferrites [6 to 16]. Process IV, occurring near 200 K – by comparison with corresponding relaxations observed in e^--irradiated stoichiometric magnetite [8] – is attributed to reorientations of anisotropic stress-induced interstitials of, e.g., dumbbell configuration, cf. also [9, 14].

For the ease of comparison, we have re-evaluated the most significant high-temperature spectra of the present Mn-ferrite series (Figs. 3 to 5) by means of our meantimes considerably improved analyzing techniques, cf. Section 2.3. The obtained activation parameters (cf. Table 1) compare well with the previously determined data [1].

2. Experimental Techniques

2.1 Specimen preparation

Polycrystalline Mn-ferrites, $Fe_{3-x-\Delta}Mn_xO_4$, of various composition ($2 \times 10^{-3} < x < 0.8$) have been prepared by appropriately mixing high-purity powders of Fe_2O_3 and $MnCO_3$. These mixtures, after submission to several procedures of preheating and milling, as described in detail in [1], were fired during 30 h at 1400 °C in a controlled oxygen-atmosphere of $p_{O_2} = 8 \times 10^{-4}$ atm, so as to yield in thermodynamic equilibrium a vacancy content of about $\Delta \approx 4 \times 10^{-3}$ [22, 23]. At the end of sintering, this high-temperature equilibrium was frozen in by rapidly quenching the specimens down to room-temperature.

2.2 Magnetic after-effect measurements

MAE measurements were performed within the temperature range $4.4\,\mathrm{K} \leq T < 500\,\mathrm{K}$, by means of a sensitive automated LC-oscillator technique, working in the 1 kHz range [24]. The time dependence of the reciprocal susceptibility, χ, i.e. the reluctivity $r(t,\,T) = 1/\chi(t,\,T)$, was recorded, departing from exactly 1 s (t_1) after a well-defined sample demagnetization, within the interval of $2\,\mathrm{s} \leq t_2 \leq 180\,\mathrm{s}$. Isochronal relaxation curves are plotted in form of normalized real-part differences of the complex reluctivities, as measured between t_1 and the range of ensuing times t_2:

$$\frac{\Delta r}{r_1} = \frac{\Delta r(t_1,\,t_2,\,T)}{r(t_1,\,T)} = \frac{r(t_2,\,T) - r(t_1,\,T)}{r(t_1,\,T)}\,. \tag{2}$$

This type of data representation, especially in the case of superimposed multi-process relaxations, is able to resolve the individual contributions in form of separated peaks [25]. The corresponding MAE spectra are conveniently accessible to standard numerical analyses, thus yielding high-precision values for the specific activation parameters of all participating atomistic processes ([24, 25], cf. [8, 9]).

2.3 Numerical data fitting

As described in detail previously [8, 9], each individual peak of a composed MAE spectrum (Section 2.2) is approximated by a continuous, box-type distribution of simple Debye processes with respective relaxation times $\tau_i = \tau_{0i}\,\mathrm{e}^{Q_i/\mathrm{kT}}$. Accordingly, such peaks are characterized by a central activation enthalpy, Q_i, the width of their respective enthalpy distribution, $Q_i - \Delta Q_i/2 \leq Q \leq Q_i + \Delta Q_i/2$, and a preexponential factor τ_{0i}, cf. Table 1. In order to obtain optimum least squares fitting of the spectra, the computer is allowed to approximate the various parameter sets $(Q_i,\,\Delta Q_i,\,\Delta\tau_i)$,[1]) optionally, either independently of each other – thus admitting overlap or separation of respective boxes (inset of Fig. 3b) – or in form of tight box-ranging (insets of Figs. 3a, 4, 5). The so-determined optimum process parameters of the present Mn-ferrites are compiled in Table 1.

3. Discussion of Experimental Results

3.1 Electronically induced, low-temperature MAE spectra (T < 125 K)

As novel results, with respect to our previous report [1], we present in Fig. 1 and 2, respectively, the low-temperature $(4\,\mathrm{K} < T < 200\,\mathrm{K})$ magnetic relaxation spectra and the corresponding initial susceptibility of our present series of differently Mn-doped polycrystals, together – for the ease of comparison – with the respective data obtained on stoichiometric, monocrystalline magnetite.

Thus, Fig. 1a presents the typical MAE spectrum of perfect, monocrystalline magnetite, being composed of (i) a low-temperature plateau-like relaxation regime $(4\,\mathrm{K} < T < 25\,\mathrm{K})$ which (ii) is superimposed by a thermally activated Debye-peak at

---

[1]) The forth fitting-parameter obtained by this type of analyzing technique, *the amplitude*, being representative for the *respective defect concentration* [26] – is not utilized in detail here, since presently our main interest is focussed on the observed *process mechanisms*. The numerically determined amplitudes, however, are chosen as box-heights in the insets of Figs. 3 to 5.

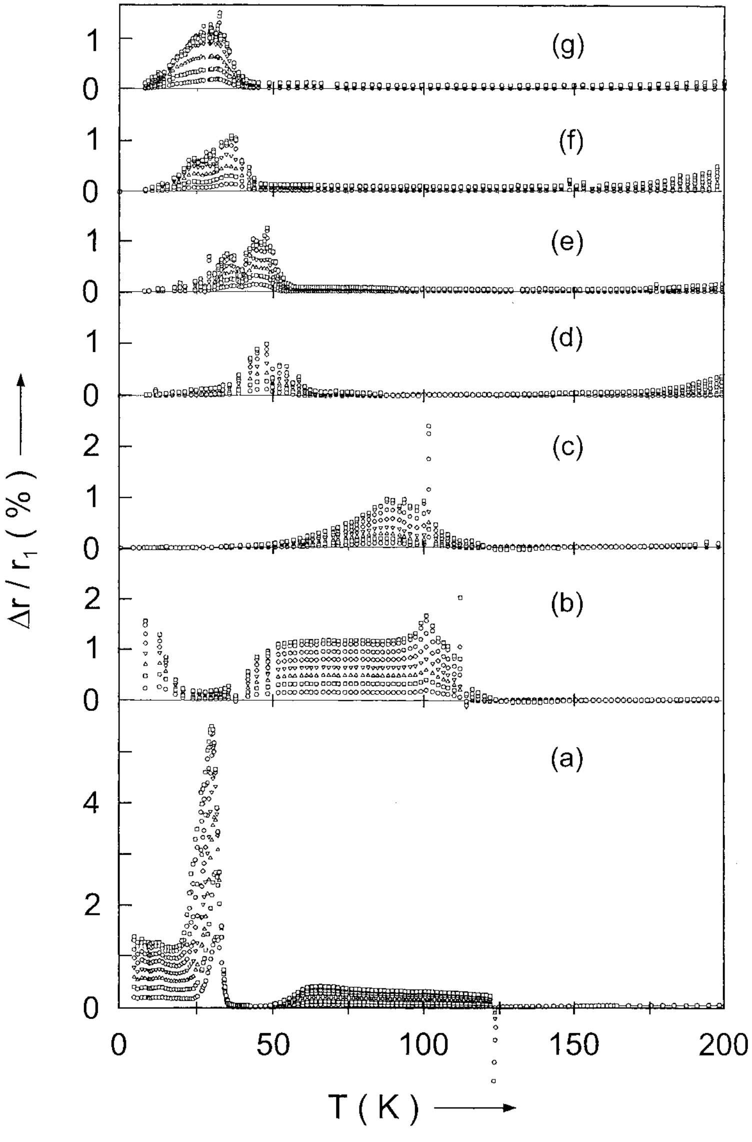

Fig. 1. Isochronal low-temperature MAE spectra of perfect, monocrystalline magnetite (a) and Mn-ferrites, $Fe_{3-x-\Delta}Mn_xO_4$, containing increasing amounts of Mn, x: 0.002 (b), 0.03 (c), 0.2 (d), 0.3 (e), 0.6 (f), 0.8 (g). The isochrones (from bottom to top) refer to measurements performed within intervals $[t_1, t_2]$, with $t_1 = 1$ s after sample demagnetization and t_2 being chosen to, respectively, 2, 4, 8, 16, 32, 64, 128 and 180 s

30 K, separated by (iii) a characteristic relaxation gap ($35\,K < T < 50\,K$) from (iv) a second plateau-like relaxation regime ($50\,K < T < 125\,K$) ending abruptly at the Verwey transition ($T_v \approx 125$ K) [3 to 8, 16].

Our preceding investigations on related ferrimagnetic systems [3 to 16] yielded the following classification for these low-temperature MAE spectra in perfect magnetite: (i)

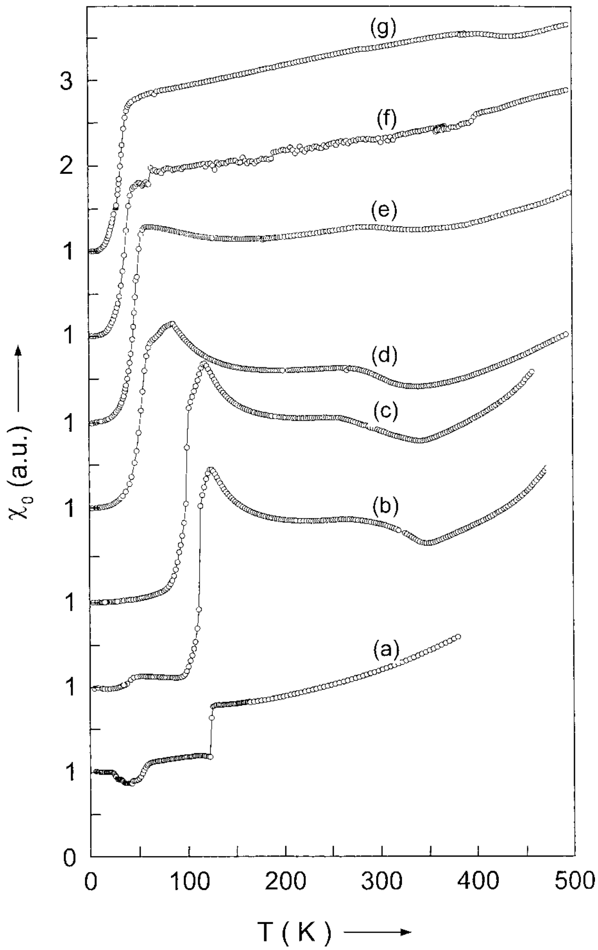

Fig. 2. Temperature dependence of the initial susceptibility of the various ferrites (a) to (g) – same notation as in Fig. 1 – containing increasing amounts of Mn

the relaxation-plateau ($4\,\mathrm{K} < T < 20\,\mathrm{K}$) is the result of long-range electron tunnelling between ordered Fe^{2+} and Fe^{3+} ions, according to (1), which, at 30 K becomes superimposed by (ii) a Debye peak, originating from thermally activated intra-atomic electronic excitations [4, 5]. (iii) The ensuing relaxation gap ($35\,\mathrm{K} < T < 50\,\mathrm{K}$), being accompanied by a pronounced drop of the initial susceptibility (Fig. 2a), signalizes freezing-in of magnetic anisotropy due to thermally induced mismatch between the tunnel-niveaus, thereby impeding any further electron exchange. At elevated temperatures ($T > 50\,\mathrm{K}$), however, renewed electron exchange according to (1) becomes enabled, in the still ionically ordered phase by (iv) thermally activated long-range electron hopping, inducing the second plateau-like relaxation regime between $50\,\mathrm{K} < T < 125\,\mathrm{K}$. Any further chance for MAE-observations of such type (1) valency fluctuations ends definitely at the Verwey transition ($T_V \approx 125\,\mathrm{K}$) where, concomitantly with a first-order crystallographic transformation from pseudo-orthorhombic to cubic, the ionic order of the low-temperature phase becomes destroyed.

As known from our preceding investigations, this MAE scenario of perfect magnetite is severely disturbed in the presence of any type of lattice defects such as, especially, ionic impurities [6 to 16], thermally quenched-in vacancies [2 to 6], irradiation-induced point defects, i.e. vacancies and interstitials [8], externally applied mechanical stress [7], etc. Thus, it was to be expected that also Mn-doping, in the additional presence of quenched-in B-site vacancies (cf. Section 2.1), would result in characteristic modifications of these low-temperature MAE spectra (cf. Fig. 1).

Typical deviations from the perfect magnetite spectrum (Fig. 1a) are observed already for smaller Mn contents ($x = 0.002$), Fig. 1b. Similarly as in other compounds, the tunnel processes react most sensibly on the presence of lattice-defects [4 to 16], as demonstrated here by a mutilated tunnel-plateau and a complete suppression of the 30 K peak. Moreover, the relaxation gap and ensuing set-in of electronic hopping, occurring here with typically increased amplitudes, are shifted to lower temperatures, as is the case also for the Verwey temperature ($T_V \approx 115$ K), cf. Fig. 2b. The minor peak near 105 K, superimposing the hopping-plateau, has been shown to result from the release of internal stresses which had been introduced during sample quenching at the end of the sinter process, cf. Section 2.2 [3 to 8, 16]. Further Mn-doping ($x = 0.03$) results in the complete suppression of the tunnel zone, a considerably retarded set-in of hopping and an enhanced low-temperature shift (104 K) of the Verwey transition (cf. Fig. 1c, 2c).

Additional details concerning the Verwey mechanism in Mn-ferrites can be deduced from inspection of their initial susceptibilities, cf. Fig. 2a to c. Whereas in perfect monocrystalline magnetite the Verwey transition gives rise to a spontaneous jump at one definite temperature (Fig. 2a), the corresponding transitions in defect-induced specimens appear less sharp, being escorted by typical low- and high-temperature tails. The corresponding low-temperature tails, evidently, result from the above-mentioned stress-release and are regarded as indicators of the higher-order nature of these respective transitions. The high-temperature tails, on the other hand, being characterized by temperature-shifted cusps superimposing the spontaneous jumps (cf. Fig. 2b to d), are associated with a correspondingly retarded zero-crossing of the crystal anisotropy constant K_1. This effect is known to occur especially in Co-doped magnetites [17, 27], where we have studied it in great detail, too, with our MAE technique [28].

Another interesting feature is the different temperature-dependence of the initial susceptibility above the Verwey transition in perfect monocrystalline and disturbed polycrystalline magnetites: whereas in the former, the once attained value is kept and only slowly increased upon further heating (Fig. 2a), the latter are characterized by a certain susceptibility drop after the zero-passing of the anisotropy (Fig. 2b to d). Upon further Mn-doping ($0.2 \leq x \leq 0.8$) the character of the low-temperature MAE spectrum becomes drastically changed into a residual, further narrowed hopping-like relaxation zone which, proportional to Mn-doping, is continuously shifted to lower temperatures ($T \leq 50$ K), Interestingly, the upper-temperature decay of this deformed relaxation zone is accompanied by a correspondingly broadened jump of the susceptibility with almost doping-invariant amplitudes, cf. Fig. 2b to g. Especially this latter item leads us to regard these low-temperature spectra as emerging from hopping processes within reduced temperature regimes, becoming suppressed at their upper end by second-order, Verwey-like, crystallographic transformations. Astonishingly, these transformations are accompanied by almost Mn-independent anisotropy reductions being accompanied by corresponding increments of the domain-wall mobility (susceptibility) in the differently

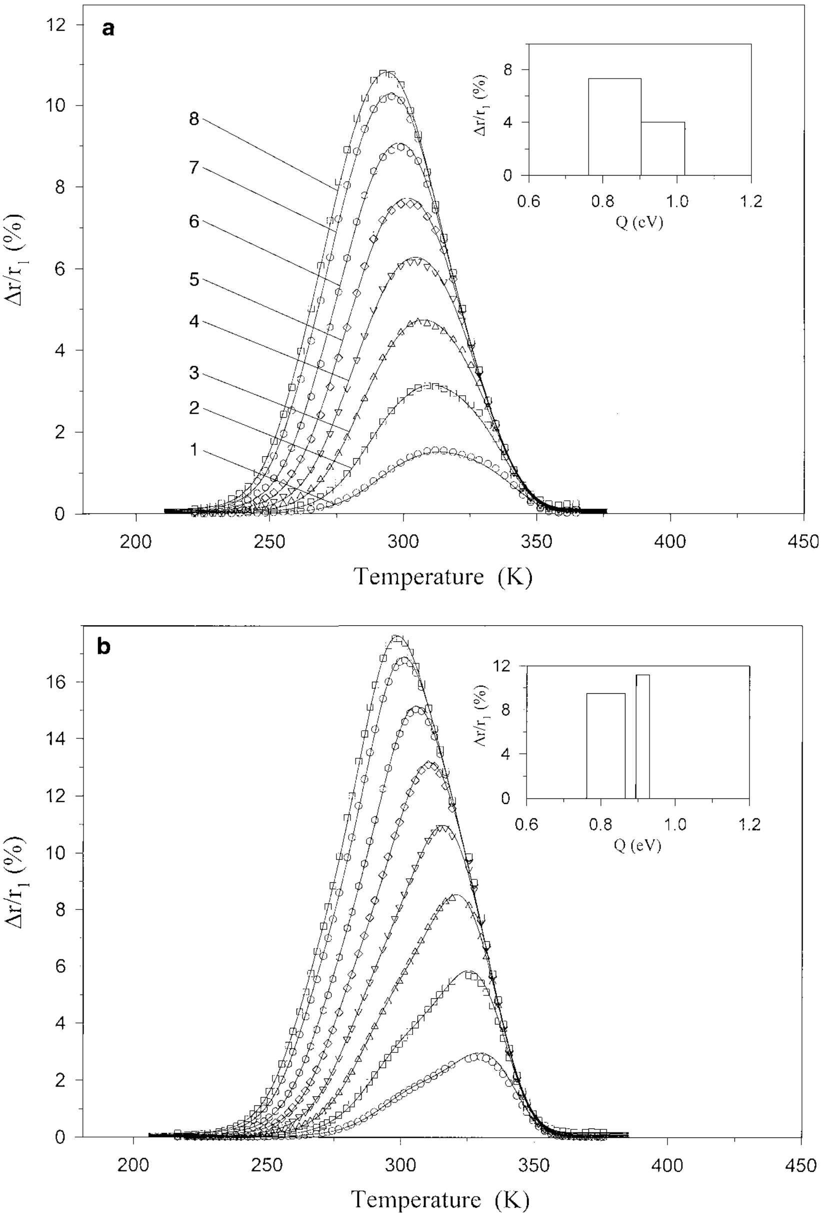

Fig. 3. a) Fitting of peak III in high-purity, vacancy-doped magnetite $Fe_{3-\Delta}O_4$ ($\Delta = 3 \times 10^{-4}$), serving as reference for the following relaxations obtained in differently Mn-doped magnetites; symbols and continuous lines correspond, respectively, to experimental data and numerical approximation. The measuring times of the tagged isochronals are identical with those described in Fig. 1, i.e., $t_1 = 1$ s and $t_2 = 2$ s (1), 4 s(2), 8 s(3), 16 s(4), 32 s(5), 64 s(6), 128 s(7) and 180 s(8). The inset shows the computer-determined box-type distributed enthalpy spectrum which governs the observed relaxation processes, cf. Section 2.3. b) Fitting of peak III, including the respective enthalpy spectrum (inset), of $Fe_{3-x-\Delta}Mn_xO_4$ ($x = 0.002$). Symbols, lines and measuring times correspond to those of Fig. 3a

doped samples. In no other ferrimagnetic material investigated so far, we have observed comparable Verwey-like crystallographic transformations to remain active over such wide ranges of impurity doping, thereby undergoing such extreme low-temperature shifting, accompanied by almost unvaried susceptibility jumping.

3.2 Vacancy-mediated ionic relaxation processes III and II

These types of magnetic relaxation processes occurring above the Verwey transition, in the temperature range 200 K $< T <$ 500 K, have been studied to all details in our preceding report [1] so that, to their respect, we can confine us here on a short summary of the previous discussion. For the sake of completeness, we have re-evaluated the most

Table 1

Compilation of representative, numerically determined activation parameters of processes III (III_1, III_2), II (II_1, II_2) and IV for the present Mn-ferrites, in dependence on varying Mn contents, x. The tagged data rows for Mn contents of $x = 0.6$ may indicate that in this case optimum approximation of peak III and II was achieved by superposition of only three, instead of four, subprocesses with correspondingly increased latitudes ΔQ of their enthalpy spectra

process	T (K)	x	Q (eV)	ΔQ (eV)	τ_0 (10^{-14} s)	source/ Fig.
tunnelling	≤4 to 20	0.0000	0.031	0.046	10^4	[6, 8] 1a
	30	0.0000	0.06 0.08	0.017/ 0.013	68×10^3 1.4×10^3	[6, 8] 1a
hopping	50 to 125	0.0000	0.25	0.18	10^2	[6, 8] 1a
III_1	≈280	0.0000	0.82	0.14	9.6	[6, 8, 15] 3a
		0.002	0.81	0.10	12	3b
		0.03	0.80	0.10	8	4a
		0.20	0.80	0.14	16	4b
		0.30	0.81	0.14	24	5a
		0.60	0.76	0.20	57	5b
III_2	≈300	0.0000	0.95_6	0.12	0.1_7	[6, 8, 15] 3a
		0.002	0.91	0.04	12	3b
		0.03	0.88	0.06	8	4a
		0.20	0.93	0.12	24	4b
		0.30	0.94	0.14	46	5a
		*0.60	0.95	0.26	120	5b
II_1	≈380	0.0000	–	–	–	3a
		0.002	–	–	–	3b
		0.03	–	–	–	4a
		0.20	1.05	0.12	92	4b
		0.30	1.08	0.12	100	5a
		*0.60	0.95	0.26	120	5b
II_2	>400	0.0000	–	–	–	3a
		0.002	–	–	–	3b
		0.03	–	–	–	4a
		0.20	1.21	0.20	100	4b
		0.30	1.21	0.14	100	5a
		0.60	1.17	0.20	108	5b
IV	≈200	0.60	0.60	0.20	57	5b

prominent peaks of these spectra, using state-of-the-art evaluation techniques (cf. Section 2.3, Figs. 3 to 5), and compiled the obtained data – which are in fair agreement with the previous results – in Table 1.

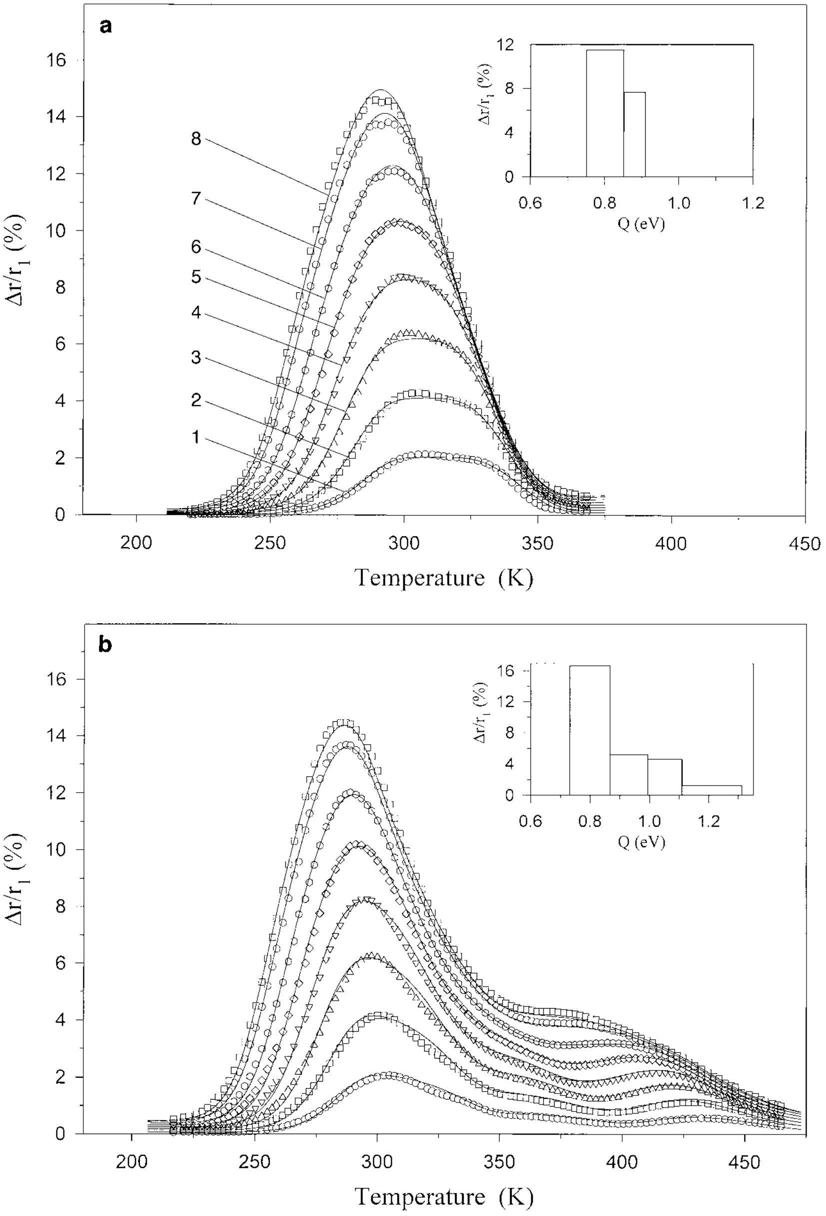

Fig. 4. a) Fitting of peak III, including the respective enthalpy spectrum (inset), in $Fe_{3-x-\Delta}Mn_xO_4$ ($x = 0.03$). Symbols, lines and measuring times correspond to those of Fig. 3a. b) Fitting of peaks III and II, including their respective enthalpy spectra (inset), in $Fe_{3-x-\Delta}Mn_xO_4$ ($x = 0.2$). Symbols, lines and measuring times correspond to those of Fig. 3a

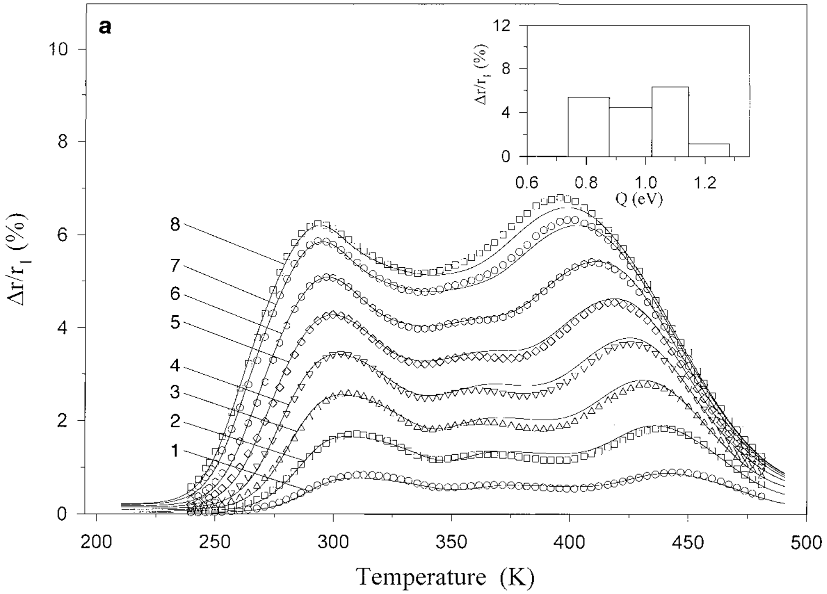

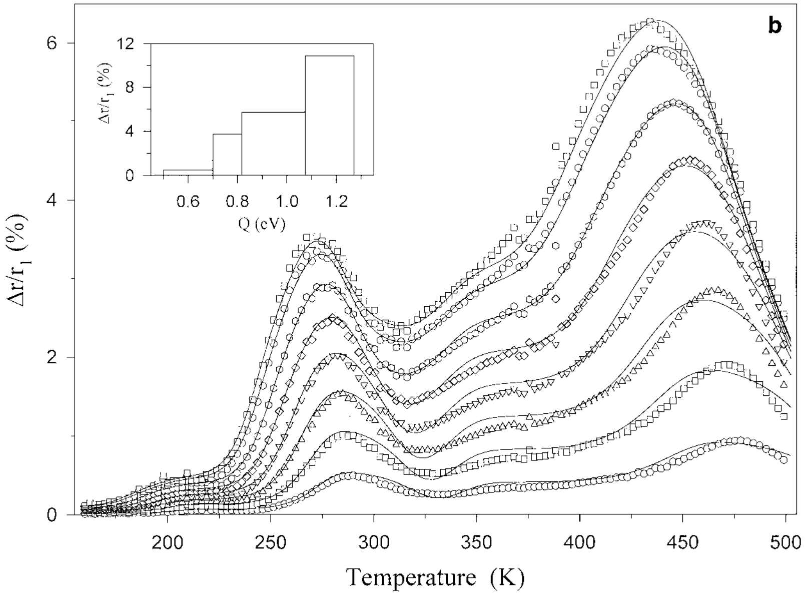

Fig. 5. Fitting of peaks III and II, including their respective enthalpy spectra (inset), in $Fe_{3-x-\Delta}Mn_xO_4$ ($x = 0.3$). Symbols, lines and measuring times correspond to those of Fig. 3a. b) Fitting of peaks III and II, including their respective enthalpy spectra (inset), in $Fe_{3-x-\Delta}Mn_xO_4$ ($x = 0.6$). Symbols, lines and measuring times correspond to those of Fig. 3a

3.2.1 Basic relaxation model III in pure, vacancy-doped magnetite

The prototype of all vacancy-mediated ionic relaxation processes in magnetite-based compounds may be seen in process III, occurring near 300 K in pure magnetite containing octahedral (B-site) vacancies, cf. Fig. 3a [2 to 16]. The analysis of this peak reveals it to be composed of at least two subprocesses, the mechanisms of which are depicted in Fig. 6: Due to the local Fe-ion distribution around a B-site vacancy, i.e. in form of the two triplets B_1 and B_2, the vacancy site is exposed to a trigonal $\langle 111 \rangle$ lattice distortion. This local anisotropy may be lifted if – by interaction with the residual orbital momentum of a neighboured Fe^{2+} ion – this ion undergoes a thermally activated jump into the vacancy. Due to this local anisotropy variation the interaction with the domain walls becomes modified, too, thus giving rise to a magnetic after-effect. According to Fig. 6, two modes of Fe^{2+}-jumping are to be envisaged: (i) jumping of an as-ready Fe^{2+} ion (B_1), or jumping of an Fe^{2+} ion formed of an Fe^{3+} ion, which before had to capture a hopping electron (B_{2a}).

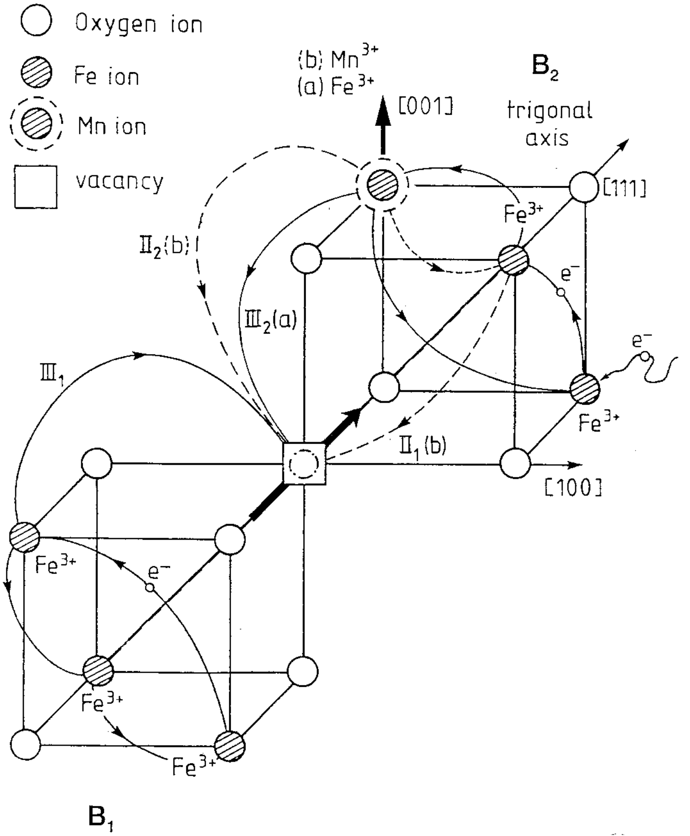

Fig. 6. Relaxation model illustrating the mechanisms of (a) subprocesses III_1, III_2 of process III in high-purity magnetite due to jumping of Fe^{2+} ions from B_1- and B_2-type triplets into an octahedral (B-site) vacancy and (b) the additionally occurring processes II_1 and II_2 in Mn-doped magnetite (dashed lines), induced by corresponding jumps of Jahn-Teller stabilized Fe^{2+} and Mn^{3+} ions from (B_2) into the vacancy

The enthalpies of these two modified jump mechanisms differ by the enthalpy of electron hopping, of about 0.1 eV [17 to 19, 29], thus giving rise to the formation of two closely overlapping relaxation maxima, as deduced also from the analysis of the 300 K peak, cf. Table 1, Fig. 3a.

3.2.2 Processes III and II in Mn-ferrite revisited

Typically, in all vacancy-doped magnetite-based ferrites the admixture of ionic impurities causes a splitting of the fundamental process III into higher-temperature (II) and, frequently also, lower-temperature (IV) satellites [9 to 16]. This rule is also obeyed by our present vacancy-doped magnetites (Figs. 3 to 5 and Fig. 7): in dependence on continued Mn-substitution ($0 < x < 0.8$), we observe – concomitantly with the decrease of the 300 K amplitude – a successive growth of peak II (Fig. 7a). This satellite, in turn, proves to be composed of two subprocesses (Table 1) whose effective maximum, in dependence on Mn content, is shifted to higher temperatures, within the range $370\text{ K} < T < 450\text{ K}$, Fig. 7b. Continued Mn-doping, in addition, leads to the occurrence and moderate growth of process IV near 200 K (cf. Fig. 5b, [1]). Based on our interpretations developed in [1], the formation and further reaction of process II can be summarized as follows:

(i) As a basic feature of Mn-doping we have to keep in mind that $Fe_{3-x-\Delta}Mn_xO_4$, for increasing contents x, undergoes a gradual change from an inverse ($x = 0$) into a normal spinel, attaining for $x = 1$ – i.e. stoichiometric Mn ferrite – a degree of about 80% normality [17 to 19, 30].

(ii) Mn, entering initially the spinel lattice as divalent ion (Mn^{2+}) is supposed to reside in this state when substituted on A-sites, but to vary between Mn^{2+} and Mn^{3+} on

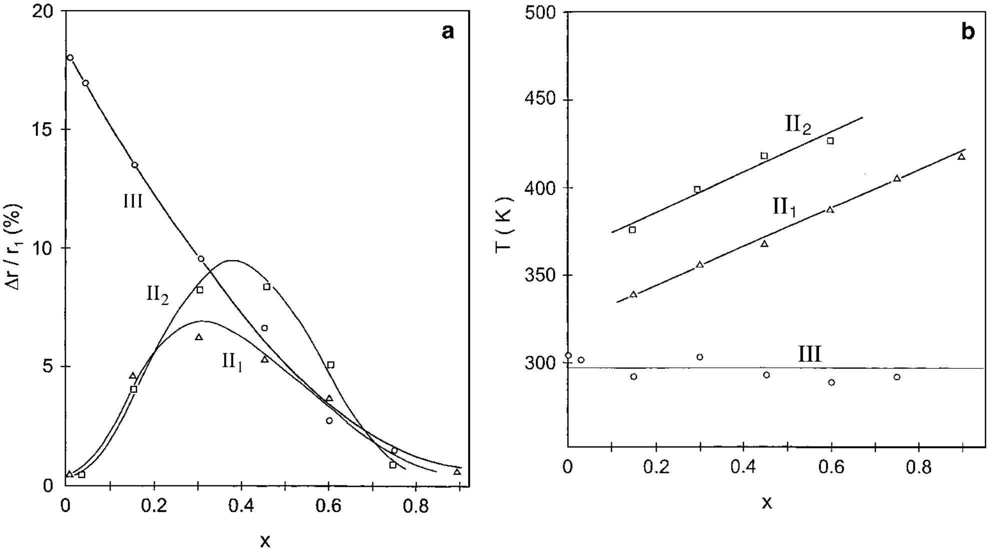

Fig. 7. a) Amplitude dependence of the composed process III and subprocesses II_1, II_2 on increasing Mn contents ($t_1 = 1$ s, $t_2 = 180$ s), cf. [1]. b) Temperature shift of the maxima of the composed process III and subprocesses II_1, II_2 in dependence on increasing Mn contents ($t_1 = 1$ s, $t_2 = 180$ s), cf. [1]

B-sites due to electron exchange between neighboring Fe ions, Fig. 6 (b):

$$Mn^{2+}Fe^{3+} \leftrightarrows Mn^{3+}Fe^{2+} . \tag{3}$$

With increasing Mn content, the equilibrium of (3) is expected to become shifted to the right, where a Jahn-Teller induced tetragonal distortion is able to lift the degenerate $3d^4$ ($d\varepsilon^3$ $d\gamma^1$) electronic groundstate of the Mn^{3+} ion, thereby stabilizing, by interaction of the local lattice with the orbital ionic anisotropy, the formation of the $Mn^{3+}Fe^{2+}$ pair (cf. configuration B_2 in Fig. 6). Evidently, Fe^{2+} ions engaged in such pairs need higher thermal activation for jumping into the B-site vacancy (cf. process II_1 in Fig. 6), i.e. with the standard enthalpy of $Q_0 \approx 0.88$ eV increased by the additional Jahn-Teller induced binding enthalpy of $0 < Q_B < 0.4$ eV [1, 31] (Table 1), than Fe^{2+} ions jumping with the modi III_1 and III_2, cf. Fig. 6. The second, higher-activated subprocess II_2 of peak II is attributed to a modified, also vacancy-mediated ionic diffusion of Mn^{2+} instead of Fe^{2+} ions [1].

This model, being fully developed in [1], is able to explain the observed variations of peaks III and II in dependence on continued Mn-doping (cf. Fig. 7a, b): Clearly, increasing Mn substitution has the combined effect of a) to rise the number of Jahn-Teller induced $Mn^{3+}Fe^{2+}$ pairs thereby strengthening process II, at least initially – up to contents of about $x \approx 0.4$ [1] – and b) to correspondingly lower the amount of undisturbed B_1 site triplets, thereby reducing the amplitude of process III (Fig. 7a). The concomitant shift of peak II to higher temperatures (Fig. 7b) is attributed to enforced ionic pair-binding, supported by collective interactions between the augmenting centres of local anisotropy [19, 32], thus affecting both subprocesses of peak II in a similar way [1].

Upon Mn-doping to contents above $x = 0.4$ the amplitude of process III continues to further drop, being accompanied in this tendency now, however, by both sub-components of satellite II (Fig. 7a) [1]. These observations are attributed to extended Jahn-Teller induced $Mn^{3+}Fe^{2+}$-pair clustering in combination with enhanced redistribution of Mn^{2+} ions onto A-sites, thus causing a) further reduction of the number of B-sited, two-valent ions (Fe^{2+} and Mn^{2+}) and b) an increase of their activation enthalpies due to enhanced pair-binding.

3.2.3 Intrinsic interstitial-type relaxation IV

As regards process IV, which develops near 200 K upon continued Mn-doping, we are able here to give a more detailed interpretation than in [1]. This is based on the observation of a corresponding 200 K relaxation occurring in e^--irradiated, monocrystalline magnetite, where this process could be definitely associated with the reorientation of anisotropic intrinsic interstitial-type defects [8]. Similarly, we could identify corresponding 200 K peaks in the MAE spectra of Ba- [9] and Ti-doped [14] magnetite as being of an intrinsic interstitial reorientation type. In these latter two compounds the occurrence of process IV has been attributed to oversized ions, incorporated into the spinel lattice either by direct substitution (Ba^{2+}) or by substitution-dependent valency variations (Ti^{4+}). Thus, in the latter case, Ti^{4+} is exclusively inserted on octahedral lattice sites thereby inducing – by reasons of charge neutrality – a corresponding number of B- and A-sited Fe^{3+} ions to change their valency into Fe^{2+} [14]. Due to the increased ionic radius of Fe^{2+} (0.84 Å) as compared to Fe^{3+} (0.64 Å) [33], this valency change is accompanied by internal stresses – being further enhanced by Jahn-Teller induced cooperative ordering of the residual Fe^{2+} orbital moments. Under the action of these stresses, Fe ions are expected to become displaced from their normal lattice sites into dumb-bell-like interstitial positions [14] where, after thermal activation near 200 K, they give rise to the reorientation-type process IV.

In the case of Mn-doped magnetite we have the similar situation that, upon continued Mn substitution, A-sited Fe^{3+} ions (radius: 0.64 Å) are increasingly replaced by Mn^{2+} (0.83 Å) which due to their larger diameters [33] present sources of internal stress. These stresses, again, are expected to be further enhanced by the Jahn-Teller induced B-site lattice distortions, originating from the formation of anisotropic $Mn^{3+}Fe^{2+}$ pairs. Thus, like in the case of Ti-ferrite, we suppose these stresses to produce intrinsic interstitials,[2]) i.e. by forcing Fe ions into dumb-bell configurations, being responsible for the occurrence of the reorientation-type process IV near 200 K [8, 9, 14].

4. Summary

1. Special emphasis has been laid on the investigation of the low-temperature ($T < 125$ K) electronic MAE processes. Whereas tunnelling is severely affected, departing already from lowest Mn contents ($x \leq 0.002$), hopping is observed over the whole range of Mn doping, up to $x \leq 0.8$, though in more and more mutilated modes, being finally shifted to temperatures <50 K.

2. Like in perfect magnetite, the high-temperature end of hopping is accompanied – over the whole concentration range – by a pronounced, almost strength-invariant susceptibility jump, indicating a concentration-dependent change from first to second or higher order. This behaviour is in contrast to most other magnetite-based ferrites where the impingement of hopping, in connection with continued doping, is reflected by a gradual suppression of corresponding suceptibility jumps. The exceptional performance of Mn-ferrite, in our eyes, is indicative for the preservation of a certain Verwey-like order transition – even up to high Mn contents – due to a corresponding order stabilization by means of Jahn-Teller-induced local anisotropies around B-sited Mn^{3+} ions.

3. The MAE spectra of the vacancy-mediated ionic processes III and II have been quantitatively analyzed and their dependence on the Mn substitution discussed in terms of a B-site vacancy model being specifically modified by the Jahn-Teller effect of neighboring Mn^{3+} ions.

4. Process IV, occurring near 200 K, is interpreted in a novel way as being induced by reorientations of anisotropic intrinsic interstitial configurations of, e.g., dumb-bell type. These interstitials are expected to be formed under the influence of internal stresses resulting – upon increasing Mn doping – from exchange of A-sited Fe^{3+} by higher-voluminous Mn^{2+} ions, in addition to enhanced Jahn-Teller distortions around B-sited Mn^{3+} ions.

---

[2]) This interpretation is further supported by a second series of measurements performed in [1], where in samples of constant Mn content ($x = 0.45$) the vacancy concentration has been systematically increased ($0 < \Delta < 5 \times 10^{-2}$). At elevated vacancy contents, again, the occurrence of process IV is observed which, also in this case, can be attributed to valency-dominated replacements of A-sited Fe^{3+} by Mn^{2+} ions, being accompanied by the production of stress-induced intrinsic interstitials.

References

[1] F. Walz and J. Rivas, phys. stat. sol. (a) **37**, 151 (1976).
[2] H. Kronmüller, R. Schützenauer, and F. Walz, phys. stat. sol. (a) **24**, 487 (1974).
[3] F. Walz, H. Deusch, and H. Kronmüller, phys. stat. sol. (a) **53**, 519 (1979).
[4] F. Walz, M. Weidner, and H. Kronmüller, phys. stat. sol. (a) **59**, 171 (1980).
[5] H. Kronmüller and F. Walz, Phil. Mag. **B42**, 433 (1980).
[6] F. Walz, V. A. M. Brabers, S. Chikazumi, H. Kronmüller, and M. O. Rigo, phys. stat. sol. (b) **110**, 471 (1982).
[7] F. Walz and H. Kronmüller, Phil. Mag. **B64**, 623 (1991).
[8] F. Walz and H. Kronmüller, phys. stat. sol. (b) **160**, 661 (1990); **181**, 485 (1994).
[9] F. Walz, J. Rivas, D. Martínez, and H. Kronmüller, phys. stat. sol. (a) **143**, 137 (1994); **144**, 177 (1994).
[10] F. Walz, J. Rivas, J. Iñiguez, and H. Kronmüller, phys. stat. sol. (a) **151**, 435 (1995); **158**, 217 (1996).
[11] L. Torres, F. Walz, C. de Francisco, and J. Iñiguez, phys. stat. sol. (a) **163**, 221 (1997).
[12] F. Walz, L. Torres, C. de Francisco, J. Iñiguez, and H. Kronmüller, phys. stat. sol. (a) **163**, 233 (1997).
[13] L. Torres, F. Walz, K. Bendimya, C. de Francisco, and H. Kronmüller, phys. stat. sol. (a) **161**, 289 (1997).
[14] F. Walz, J. Torres, K. Bendimya, C. de Francisco, and H. Kronmüller, phys. stat. sol. (a) **164**, 805 (1997).
[15] F. Walz and V. A. M. Brabers, phys. stat. sol. (a) **156**, 471 (1996); **168**, 281 (1998).
[16] F. Walz, V. A. M. Brabers, and H. Kronmüller, J. Physique IV **7**, C1-569 (1997).
[17] J. Smit and H. P. J. Wijn, Ferrite, Philips Technische Bibliothek, Eindhoven (Holland) 1959.
[18] S. Chikazumi, Physics of Magnetism, R. E. Krieger Publ. Co., Huntington/New York 1978.
[19] V. A. M. Brabers, in: Handbook of Magnetic Materials, Ed. K. H. J. Buschow, Vol. 8, North-Holland Publ. Co., Amsterdam 1995 (Chap. 3).
[20] J. H. V. J. Brabers, F. Walz, and H. Kronmüller, Physica B **266**, 321 (1999).
[21] N. Lenge, H. Kronmüller, and F. Walz, J. Phys. Soc. Japan **53**, 1406 (1984).
[22] L. S. Darken and R. W. Gurry, J. Amer. Chem. Soc. **67**, 1398 (1945); **68**, 798 (1946).
[23] H. Schmalzried and J. D. Tretjakow, Z. Elektrochem. (Ber. Bunsenges. Phys. Chem.) **70**, 180 (1966).
[24] F. Walz, phys. stat. sol. (a) **8**, 125 (1971); Appl. Phys. **3**, 313 (1974); phys. stat. sol. (a) **82**, 179 (1984); phys. stat. sol. (a) **147**, 237 (1995).
[25] H. Kronmüller, Nachwirkung in Ferromagnetika, Springer-Verlag, Berlin/Heidelberg/New York 1968.
[26] F. Walz, M. Weller, and M. Hirscher, phys. stat. sol. (a) **154**, 765 (1996).
[27] L. R. Bickford, J. M. Brownlow, and R. F. Penoyer, Proc. IEE B **104**, 238 (1957).
[28] F. Walz and V. A. M. Brabers, to be published.
[29] R. Dieckmann, C. A. Witt, and T. O. Mason, Ber. Bunsenges. Phys. Chem. **87**, 495 (1983).
[30] J. M. Hastings and L. M. Corliss, Phys. Rev. **104**, 328 (1956).
[31] S. Krupička and K. Záveta, J. Appl. Phys. **39**, 930 (1968).
[32] Z. Šimša and J. Šimšowá, Czech. J. Phys. **B24**, 439 (1974).
[33] R. D. Shannon, Acta Cryst. **A32**, 751 (1976).